Microviscosity in Multiple Regions of Complex Aqueous Solutions of Poly(ethylene oxide)−Poly(propylene oxide)−Poly(ethylene oxide)

Christian D. Grant, Karen E. Steege,† Michelle R. Bunagan,‡ and Edward W. Castner, Jr.*

Department of Chemistry and Chemical Biology, Rutgers, The State University of New Jersey, 610 Taylor Road, Piscataway, New Jersey 08854-8087

Received: July 17, 2005; In Final Form: September 20, 2005

Aqueous poly(ethylene oxide)−poly(propylene oxide)−poly(ethylene oxide) ($PEO_{109}-PPO_{41}-PEO_{109}$) copolymers are nonionic surfactants that self-organize to form aggregate structures with increasing temperature or concentration. We have studied two concentrations over a range of temperatures so that the copolymers are in one of three microphases: unimers, micelles, or hydrogels formed from body centered cubic aggregates of micelles. Three different coumarin dyes were chosen based on their hydrophobicity so that different aggregate regions could be probed independently—water insoluble coumarin 153 (C153), hydrophobic coumarin 102 (C102), and the hydrophilic sodium carboxylate form of coumarin 343 ($C343^-$). Fluorescence anisotropy experiments provide detailed information on the local microviscosity. C153 experiences a fourfold increase in reorientation time and hence microviscosity with increasing temperature through the microphase transition from unimers to micelles. C102 also shows an increase in microviscosity with temperature but smaller in magnitude and with the microphase transition shifted to higher temperature relative to C153. $C343^-$ shows only a slight sensitivity to the microphase transition. For any of the three coumarin probes, fluorescence anisotropies do not show any correlation with the microphase transition to form cubic hydrogels.

Introduction

A detailed understanding of specific interactions or local friction in complex solutions is essential for optimizing chemical and physical processes on the nanometer scale such as drug delivery, nanoparticle synthesis, and molecular aggregation phenomena in general. Fluorescence polarization anisotropy experiments directly probe orientational motions, thereby measuring the local friction or microviscosity on the relevant molecular length scales. Microviscosity is the friction experienced by a solute molecule at the microscopic scale; it is an important parameter for characterizing the local environment because modest changes in local viscosity lead to variable diffusion rates and hence chemical reaction rates.

A−B−A triblock copolymers of poly(ethylene oxide)−poly(propylene oxide)−poly(ethylene oxide) (PEO−PPO−PEO) are nonionic surfactants that have interesting and unique properties.[1] These PEO−PPO−PEO triblock copolymers are commercially available from several manufacturers (including BASF, Dow, ICI, and Serva) and have broad industrial uses that include foaming, detergency, lubrication, and emulsification applications. They have also been tested as controlled drug encapsulation and delivery systems because of their low toxicity and amphiphilic nature.[2−4]

Solutions of PEO−PPO−PEO copolymers show complex behavior.[5] As many as nine phases have been identified as either concentration and/or temperature are varied in a ternary system of water, triblock copolymer, and *p*-xylene.[6] The various microphases include unimers, spherical and rodlike micelles, several types of liquid crystals, cubic or hexagonally packed hydrogels, and lamellar aggregates.[6−8] These systems typically display microphase transitions in dilute aqueous solutions from unimers to micelles with increasing temperature.

Micellization in the PEO−PPO−PEO systems is a consequence of dehydration of the PPO block. At temperatures below 15 °C, the central PPO block is hydrated by water molecules that donate hydrogen bonds to the polyether oxygens. This leads to a hydrated random coil unimer phase for the entire triblock copolymer in solution. As the solution temperature is increased, water is no longer a good solvent for the PPO block and the PPO block dehydrates, which is the driving force for micellization. The unimer-to-micelle phase transition has been extensively studied via several techniques including small-angle neutron scattering (SANS),[9−13] NMR,[14,15] dynamic light scattering (DLS),[1,16,17] differential scanning calorimetry (DSC),[8,18−20] Fourier transform Raman and IR spectroscopies,[21] and fluorescence spectroscopy.[1,22−24] Our recent fluorescence studies using coumarin dyes via time-integrated and time-resolved fluorescence measurements on Pluronic F88 corroborate the known details of the micellization microphase transition occurring at 34 °C for 5 w/v % and 22.5 °C for 25 w/v %.[25]

Micelle−micelle entanglement (PEO interpenetrating between micelles) at higher concentrations of PEO−PPO−PEO solutions leads to solution gelation with increasing temperature.[5,13−15,26−28] The gel breaks down or melts at higher temperatures because of micellar structural changes such as the elongation of spherical micelles to form rodlike micelles.[7] The solution cloud point occurs when the PEO chains are fully dehydrated. The 25 w/v % aqueous solutions of $poly(ethylene\ oxide)_{109}-poly(propylene\ oxide)_{41}-poly(ethylene\ oxide)_{109}$ (Pluronic F88, $M_w \sim 12\,000$) used in this study have a sufficient micellar volume fraction of 0.53 for cubic packed spheres to gel at elevated temperatures

* To whom correspondence should be addressed. E-mail: ed.castner@rutgers.edu.

† NSF IGERT trainee in biointerfacial engineering.

‡ Née Michelle R. DeRitter. Present address: Department of Chemistry, University of Pennsylvania, 231 South 34th Street, Philadelphia, PA 19104-6323.

10.1021/jp053929k CCC: $30.25 © 2005 American Chemical Society
Published on Web 11/05/2005

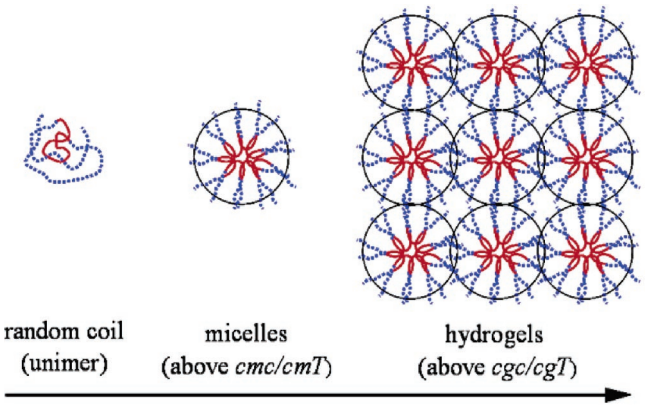

Figure 1. Schematic microphase diagram for Pluronic F88 as a function of temperature and/or concentration.[25] Aqueous 5 w/v % solutions exist as unimer and micelle solutions, while aqueous 25 w/v % F88 can form bcc cubic lattice hydrogels (far right of figure).

SCHEME 1

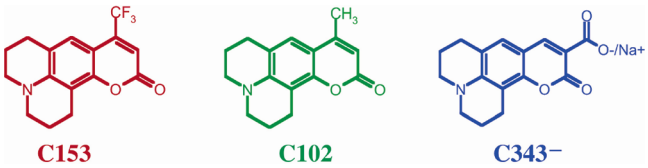

(~40 °C).[27] However, the micellar volume fraction of the 5 w/v % aqueous solutions is too low to form hydrogels. The schematic diagram in Figure 1 illustrates how random coil unimers form spherical micelles with increasing concentration and/or temperature. Body centered cubic hydrogel aggregates can be obtained at higher temperatures and concentrations.

Several varieties of PEO−PPO−PEO triblock copolymers have previously been investigated using fluorescence spectroscopy.[1,2,22−24,29−31] In particular, Jeon, et al. used the cationic dye rhodamine 123 to explore the connections between macro- vs microviscosity in 20 wt % aqueous $PEO_{100}-PPO_{65}-PEO_{100}$ (Pluronic F127) hydrogels using fluorescence anisotropy measurements.[22] Rhodamine 123 was proposed to partition into two locations, with one fraction in bulk water and the other fraction associating with the micelles.

A number of 7-aminocoumarin fluorophores display properties that make these molecules useful for dynamic probing of condensed phase environments. The three coumarin probe molecules used in the present work (see Scheme 1) have each been previously characterized in detail. Time-dependent density functional theory methods have been used previously to characterize the ground- and excited-state electronic properties of these three coumarins.[32−34] All three are relatively rigid, strongly solvatochromic, and are optimal choices for use in both solvation dynamics and local orientational friction experiments, using time-dependent fluorescence Stokes shift (TDFSS) and fluorescence anisotropy methods, respectively. In particular, coumarin 153 has been extensively characterized for use in both TDFSS and anisotropy experiments.[35,36]

For many recent studies, 7-aminocoumarins have been shown to be excellent probes of solvation dynamics and local friction.[35−40] These coumarin molecules have been used for probing complex environments including polymers,[41,42] reverse[43−50] and normal micelles,[51,52] sol−gels,[53] vesicles,[54] proteins,[55] cyclodextrins,[56] molten salts,[57] zeolites,[58] drug-delivery polymers,[59] and room-temperature ionic liquids.[60−64] Recently, Shirota et al. studied the fluorescence dynamics of C102 and C153 inside SDS micelles.[65] In this work, the same qualitative results were obtained for both probes in the SDS micelle interiors,[65] as the range of environments in which the hydrophobic probe molecules can partition is not as heterogeneous as in the present case of the triblock copolymer aqueous aggregates.

Although C153, C102, and $C343^-$ share very similar molecular geometries, volumes, and spectroscopic characteristics, they have greatly varying hydrophobicities. By selecting coumarin fluorescence probe molecules with different solubilities, we demonstrated that we can probe different local environments in PEO−PPO−PEO triblock copolymer solutions in three different phases: random coil (unimer) solutions, micellar solutions, and solid micellar hydrogel solutions. One way of quantifying the relative hydrophobicity of the three heteroaromatic coumarin probes is to invoke a method widely used in the pharmaceutical industry, which is to calculate the log of the octanol−water partition coefficient, or CLOGP.[66] Coumarin 153 is the most hydrophobic of the three probes with a CLOGP value of 4.08. C102 has a lesser degree of hydrophobicity with a CLOGP value of 3.67. The hydrophilic sodium salt of coumarin 343 is estimated to have a CLOGP value of −1.09. This explains the propensity for the $C343^-$ to probe aqueous phases and for C153 and C102 to probe hydrophobic regions. Experimentally, C102 is sparingly water soluble, while C153 is water insoluble, indicating that the difference between the true log *P* values for C153 and C102 is actually larger than these calculated estimates. Figure 2 illustrates how C153 will localize in the hydrophobic core of the micelle, while C102 will localize in the core but near the PPO−PEO interface. $C343^-$ is shown to be directly exposed to the bulk aqueous solution, with some fraction near the hydrated PEO corona of the micelles.

Microviscosities have been obtained for multiple environments within unimer, micelle, and hydrogel solutions of PEO−

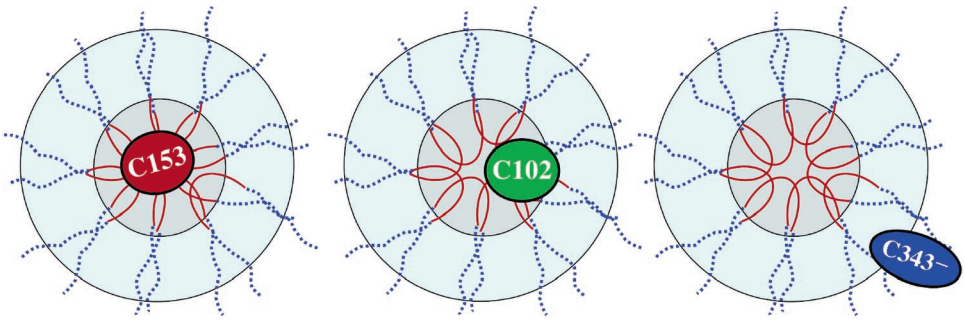

Figure 2. Diagram depicting possible coumarin dye probe locations in the F88 triblock copolymer micelles. The ellipsoidal coumarin dye representations reflect the approximate shape of the actual molecule.

PPO−PEO triblocks by means of fluorescence anisotropy measurements. Using the three coumarins, we will show how the effective local viscosity differs from the dynamic macroscopic viscosity by a factor of up to 5×10^4. We believe that the use of a series of fluorescence probes with a substantial range of hydrophobicities can become a general method for probing local friction and solvation in complex local environments, such as aggregates, proteins, and porous nanomaterials.

Experiments and Methods

Sample Preparation. Pharmaceutical grade poly(ethylene oxide)$_{109}$−poly(propylene oxide)$_{41}$−poly(ethylene oxide)$_{109}$ (Pluronic F88) samples were a gift from BASF and were used as received. Polymer solutions were prepared using 0.05 or 0.25 g of Pluronic F88 per 1.0 mL of Fluka Nanopure water for 5 and 25 w/v % solutions, respectively. Solutions were magnetically stirred at room temperature in a sealed container for 12 to 24 h to fully dissolve the polymer. Laser grade C153 and C102 from Kodak were used as received. Laser grade C343 was obtained from Acros Organics as the neutral acid and converted to the sodium carboxylate form by the addition of 1.1 equiv of NaOH in methanol. Crystalline $C343^-/Na^+$ was recovered after methanol evaporation. Fluorescence samples were made fresh before experiments. Coumarin concentrations were adjusted to obtain absorbance values in the range from 0.1 to 0.3 (5×10^{-6} to 1.5×10^{-5} M) at the excitation wavelength (10 mm path). The aggregation number for 5 w/v % F88 spherical micelles is 62, obtained from SANS data by Jain et al.[12] For a dye concentration of 10^{-5} M, this implies that statistically only 1 per 65 micelles will contain a coumarin probe molecule.

Time-Resolved Fluorescence Spectroscopy. Details of the time-correlated single photon counting (TCSPC) instrument have been described previously.[25,67,68] Fluorescence polarization decays were measured at different excitation (400−440 nm) and emission (478−550 nm) wavelengths depending on copolymer sample concentrations and temperatures. This wavelength selection is done to minimize distortions to the fluorescence lifetime transients that inevitably arise in the short time parts of transients for any solvatochromic probe located in a dynamically evolving polar medium,[36,37] including our aqueous samples of poly(ethylene oxide)−poly(propylene oxide)−poly(ethylene oxide). The solvent reorganization about the larger polarity excited state of the coumarin probes causes rapidly evolving fluorescence spectral dynamics that we will make substantial use of in ongoing and future work. Horng et al. have shown that the C153 fluorescence anisotropy is largely invariant with variations in the detected emission wavelength.[35] At present, we choose an emission wavelength for which there are an approximately equal number of emitting molecules contributing a fast blue-edge decay relative to those contributing a fast red-edge rise, leaving a dominant component in the emission dynamics that reflects the true excited-state lifetime.

The TCSPC transients were acquired so the peak channel contained up to 65 535 ($2^{16}-1$) fluorescence counts. Time windows of 60 or 70 ns were used to obtain the entire rise and decay profile of the fluorescent transient. Each transient was acquired with 4096 data points for a resolution of 14.6 or 17.1 ps/channel. TCSPC instrumental response profiles were obtained by scattering excitation light from an aqueous suspension of nondairy creamer using an optical density similar to that of the fluorescence samples at the excitation wavelength. The instrument response was typically ~40 ps fwhm. Transients were collected for temperatures in the range from 2.5 to 90.0 ± 0.1 °C using a Quantum Northwest TLC-50/100 thermoelectric temperature controller for the sample holder.

Data Analysis and Fitting. Fluorescence transients were fit to multiexponential models using a convolute-and-compare nonlinear least-squares algorithm. Instrument response functions were convoluted with the fluorescence decay model function $K(t)$ given by

$$K(t) = \sum_{i=1}^{n} \alpha_i \exp(-t/\tau_i) \tag{1}$$

where α_i and τ_i are the amplitude and time component, respectively, of the ith fluorescence decay.[69,70] Anisotropy fitting was done using a generalization of the simultaneous fitting procedure outlined by Cross and Fleming,[71] using macrofunctions written in Igor Pro software (Wavemetrics, Inc., version 4.09A).[72] Rather than construct the anisotropy $r(t)$, the three transients I_{VM}, I_{VV}, and I_{VH} were simultaneously fit to the equations

$$I_{VM} = K(t) \tag{2}$$

$$I_{VV} = \frac{1}{3} K(t)[1 + 2r(t)] \tag{3}$$

$$I_{VH} = \frac{1}{3} K(t)[1 - r(t)] \tag{4}$$

where the subscripts VM, VV, and VH denote vertical excitation and magic angle, vertical, and horizontal emission polarizations, respectively. The orientation time-correlation function is given by $r(t)$

$$r(t) = \sum_{i=1}^{2} r_i \exp\left(-\frac{t}{\theta_{i,\mathrm{rot}}}\right) \tag{5}$$

where r_i and $\theta_{i,\mathrm{rot}}$ are the individual amplitudes and reorientational time constants for the ith anisotropy decay, respectively. The criteria for a good fit were based upon a χ_r^2 near unity and weighted residuals having a random distribution about zero. Typical values of χ_r^2 resulting from the fit procedure are in the range from 1.01 to 1.13 for a multiexponential $K(t)$ fluorescence lifetime decay and a double-exponential anisotropy model. Though the decay of the fluorescent excited state is dominated by the intrinsic lifetime of the probe, double-, triple-, and quadruple-exponential decay laws are used to obtain the best fits, to account for the unavoidable minority decay and rise components that arise from the time-dependent fluorescence Stokes shift while using 5 nm spectral band-pass resolution on the Acton SP-150 spectrometer in the TCSPC instrument.[36,73] Anisotropy decays were also fit to a stretched-exponential model of the form $r_0 \exp[(-t/\theta_0)^\beta]$, which represents a distribution of relaxation times. As discussed in the Results and Discussion section, the double-exponential model for $r(t)$ was deemed superior to the stretched-exponential model.

Amplitude-averaged reorientation times $\langle\theta_{\mathrm{rot}}\rangle$ were calculated from the following equation

$$\langle\theta_{\mathrm{rot}}\rangle = \frac{\sum_{i=1}^{2} r_i \theta_{i,\mathrm{rot}}}{\sum_{i=1}^{2} r_i} \tag{6}$$

where r_i and $\theta_{i,\mathrm{rot}}$ are defined above.

Results and Discussion

Representative fluorescence depolarization transients are shown in Figure 3. The upper graph shows three different

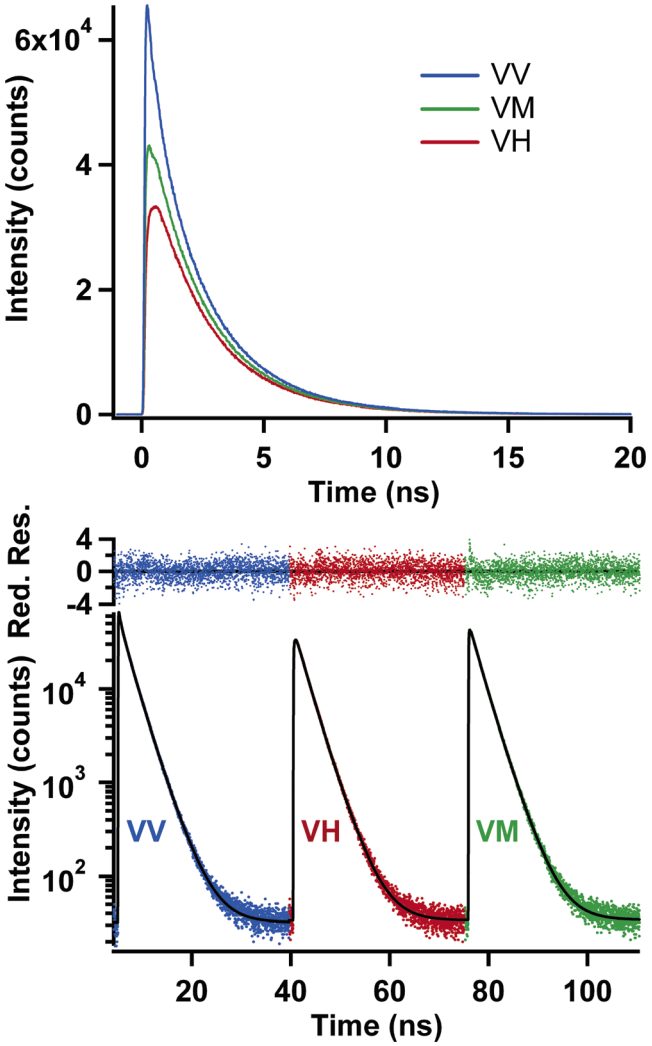

Figure 3. Representative polarization data for C153 in aqueous 5 w/v % F88 at a temperature of 7.6 °C. The top graph shows a linear stacked plot of the three different polarization transients (VV, VM, VH). This graph shows that the anisotropy fully decays on a time scale of 20 ns. The bottom part of the figure shows a simultaneous fit to the fluorescence polarization transients plotted on a semilogarithmic graph, with the reduced residuals shown in the top portion of the bottom graph for the double-exponential model. The value of χ_r^2 for the fit is 1.062.

polarizations (VV, VM, and VH) in a stacked linear plot. The utility of this representation of the data is to show that the anisotropy indeed decays fully over the time scale of our experiment. The bottom graph shows a complete data set represented as blue dots for the VV transient, red dots for the VH transient, and green dots for the VM transient. The reduced residuals are displayed at the upper end of the bottom graph and are color coded to match the polarization transients.

The transients are simultaneously fit to a multiexponential fluorescence decay model with a double-exponential anisotropy model $r(t)$. The resulting convolute-and-compare nonlinear least-squares fit is shown as a black line. We note that we also fit the anisotropy decays to a stretched-exponential model, and there is no significant difference in χ_r^2 values or reduced residuals between double- and stretched-exponential models. However, while there is no statistical difference between these fit models, the stretched-exponential fits yielded an unphysical value for the fundamental anisotropy[70] r_0 in excess of 0.4. Furthermore, it is well-known that for C153 the nonzero angle between ground- and excited-state transition dipole moments (S_o to S_1 transition) limits the fundamental anisotropy to between 0.378 in nonpolar solvents to 0.373 in polar solvents.[35] For these reasons, the double-exponential anisotropy decay model was deemed superior to the stretched-exponential model.

We believe the commonly used wobble-in-cone model[74,75] for analyzing the reorientational dynamics in other micelle and bilayer systems is not appropriate since C153 and C102 are likely not bound to an interface and do not display the behavior of a hindered rotor. The wobble-in-cone model is not appropriate for $C343^-$ because it is sampling a more bulk-like water environment. Our assumption is based on our unpublished work on reorientational dynamics of C153, C102, and $C343^-$ in poly(ethylene glycol) and poly(propylene glycol) as well as the differing solubilities for each of the coumarin dyes in these polymer melts.

Average Reorientation Time Constants and Relation to Local Friction. Aqueous Pluronic F88 solution at 5 w/v % exists mainly as random coil unimers at temperatures below 28 °C. As shown in the top graph of Figure 4, C153 exhibits a steady decrease in the average reorientation time constant $\langle\theta_{rot}\rangle$ from 361 to 255 ps over the temperature range from 2.5 to 28 °C in the aqueous 5 w/v % F88 solution. However, there is nearly a fourfold increase in the value of $\langle\theta_{rot}\rangle$ for C153 from 255 to 972 ps in the range from 28 to 38 °C. This increase in average reorientation lifetime corresponds to the unimer-to-micelle microphase transition. The C153 maps the temperature profile for the phase transition obtained from fluorescence excitation and emission spectral shifts and from the fluorescence lifetime.[25] From this maximum of 972 ps at 38 °C, $\langle\theta_{rot}\rangle$ decreases steeply to a value of 183 ps at 90 °C. C102 displays a similar decrease in the value of $\langle\theta_{rot}\rangle$ from 413 ps at 2.5 °C to 202 ps at 32 °C. This decrease in $\langle\theta_{rot}\rangle$ for C102 is followed by a jump to 449 ps at 40 °C. From 40 to 90 °C, the average C102 reorientation time constant decreases monotonically to 144 ps. The $C343^-$ also shows a steady decrease in $\langle\theta_{rot}\rangle$ from 400 to 152 ps over the range from 2.5 to 34 °C followed by a small increase to 163 ps at 38.5 °C. As the temperature increases above 40 °C, the $C343^-$ rotational time constants continue to decrease monotonically to 71 ps. It is also important to note that the increase in $\langle\theta_{rot}\rangle$ signifying the unimer-to-micelle microphase transition occurs at a higher temperature for C102 and $C343^-$ than for C153.

A similar set of temperature responses for $\langle\theta_{rot}\rangle$ is obtained for C153, C102, and $C343^-$ in the 25 w/v % aqueous F88 solution but with the microphase transition from unimers to micelles observed at a lower temperature. Coumarin 153 in aqueous 25 w/v % F88 (bottom of Figure 4) also shows a small decrease in $\langle\theta_{rot}\rangle$ from 1028 to 724 ps in the 2.5 to 10 °C range, followed by a sharp increase to 2500 ps at 27.5 °C. A further temperature increase to 90 °C results in a significant decrease in $\langle\theta_{rot}\rangle$ from 2500 to 210 ps. C102 displays a similar decrease in $\langle\theta_{rot}\rangle$ from 876 to 464 ps between 2.5 and 20 °C that is followed by an increase to 899 ps at 28 °C. The value of $\langle\theta_{rot}\rangle$ for C102 continues to decrease for temperatures above 30 °C to a value of 130 ps at 90 °C. For $C343^-$, the value of the $\langle\theta_{rot}\rangle$ decreases from 942 ps at 2.5 °C to 420 ps at 23 °C. There is a slight increase in $\langle\theta_{rot}\rangle$ to 444 ps at 23 °C that is followed by a steady decrease with increasing temperature to 87 ps at 90 °C for $C343^-$. Similar to the behavior observed for 5 w/v % aqueous F88, the increase in $\langle\theta_{rot}\rangle$ is shifted to a higher temperature for both C102 and $C343^-$ relative to C153. Note that the $\langle\theta_{rot}\rangle$ values for C153, C102, and $C343^-$ overlap for lower temperatures and are seen to converge as the temperature is increased toward 90 °C.

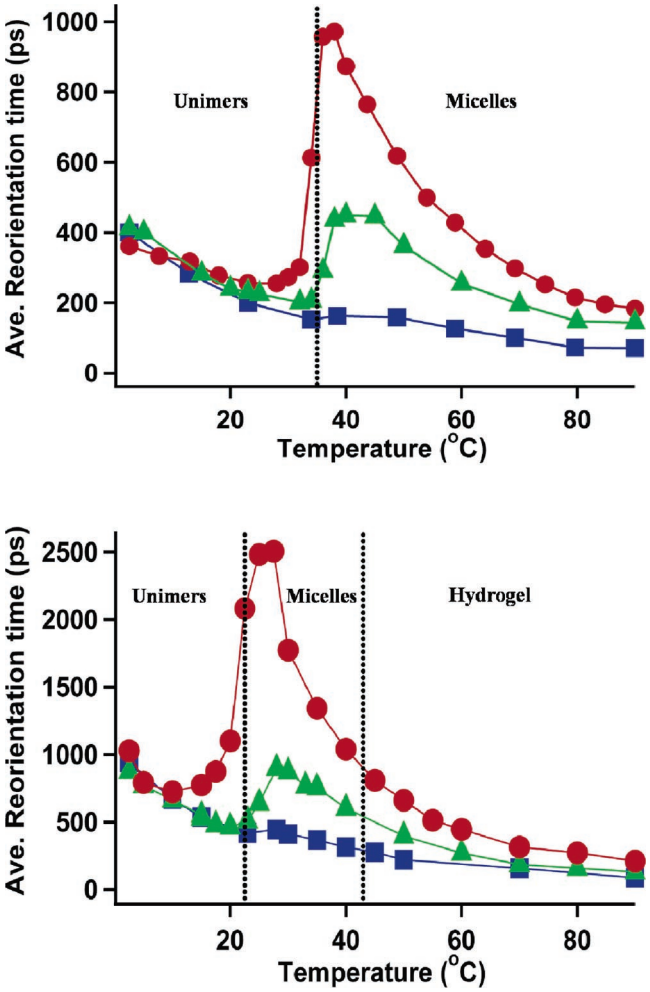

Figure 4. Temperature-dependent average reorientation times $\langle\theta_{rot}\rangle$ for C153 (red circles), C102 (green triangles), and C343$^-$ (blue squares) vs temperature: (top) 5 w/v% aqueous F88, (bottom) 25 w/v% aqueous F88. The dotted lines indicate where the microphase transitions occur. For the 5 w/v % aqueous F88 solution, the unimer-to-micelle transition occurs at 34 °C. For the 25 w/v % aqueous F88 solution, the unimer-to-micelle transition occurs at 22.5 °C while the temperature at which the solution gels is at ∼42−44 °C. The gel melting temperature is approximately 90 °C.

Figure 4 shows that for temperatures well below the critical micelle temperature (cmT), the average reorientation time constants $\langle\theta_{rot}\rangle$ for C153, C102, and C343$^-$ are superposable for 5 w/v % concentration and are also superposable for 25 w/v % concentration, albeit with a different set of values for $\langle\theta_{rot}\rangle$ for each concentration. This clearly indicates that each of the three coumarin probes localizes in an environment with the same average friction for this range of reduced temperatures in the random coil unimer solution. The steady-state excitation and emission spectra for C153, C102, and C343$^-$ have been shown to be in a water-rich environment in the lower temperature range for which F88 exists as random coil unimers in solution.[25] The emission lifetimes for C153 at these lower temperatures below the cmT are about 2.5 ns, which also indicate a wet environment.[25,67,76−78] This evidence convinces us that the C153, C102, and C343$^-$ in the unimer solution are all in a wet environment and entangled with the triblock copolymer unimers. Our reasoning that the coumarins are in contact with the polymer is based on the fact that C153 is insoluble in pure water and that the observed values for $\langle\theta_{rot}\rangle$ are at least a factor of 4 greater than one would predict from the values of water viscosity, assuming hydrodynamic scaling.[35]

At temperatures lower than the critical micelle temperature, the aqueous polymer solutions exist predominately in the unimer phase for a given polymer concentration. The cmT values for Pluronic F88 are 34 and 22.5 °C for 5 and 25 w/v % aqueous solutions, respectively. From previous time-integrated fluorescence spectra and lifetime measurements, we have deduced that, for temperatures below the cmT, C153 exists entangled with a random coil unimer in an environment similar to the PPO block. Once micellization occurs, C153 is encapsulated in the core of the micelle. Since C153 is insoluble in water, this hydrophobic probe is driven entirely into the most hydrophobic region available to it as the micellization microphase transition occurs. The C343$^-$ is extremely water soluble so it is mainly localized in a bulk water environment yet has some entanglements with unimers at low temperatures. Upon micellization, the C343$^-$ is distributed mostly in the bulk water with some fraction located in the hydrated PEO coronas. C102 behaves in a more complex manner due to its intermediate CLOGP value, entangling with unimers and associating with water at low temperatures, but likely spanning the PPO core and PPO−PEO interface. It is possible that some fraction of the C102 molecules are located in the hydrated PEO corona or even in bulk water.

The reorientation of coumarin dye probes has been studied quite extensively and has been shown to report on local environmental friction in simple and binary liquids as well as more complex fluid systems. Hence, the shift to longer average reorientation time constants for C153 and C102 upon micellization is a result of a change in the local friction. This is not an unreasonable conclusion since the micelle has a dehydrated PPO core that may be thought of as a liquid polymer droplet. Such a polymer droplet at the core of the micelle has a substantially different viscosity than the surrounding water and is in fact much like neat PPO. Thus, the coumarin fluorescence probe molecule reorientation times reflect this change in local friction. C102 behaves in a fashion similar to C153 though it is likely partitioned in at least two or more regions.

The diameters for aqueous solutions of Pluronic F88 in both micelle and random coil phases have been determined from previous studies using SANS and from DLS.[12,26] At lower temperatures, the diameter for random coils in Pluronic F88 aqueous solution is 4.2−5.8 nm as determined from SANS and DLS,[12,26] respectively. In a micelle, the micellar core, composed mainly of PPO, is estimated to be on the order of 7−10 nm depending on the degree of dehydration.[12] The diameter of the entire micelle including the PEO corona is approximately 17 nm.[12] These parameters can be used to predict the rotational diffusion time constant of a triblock copolymer random coil and micelle from hydrodynamic models. The predicted reorientation time constants can be compared with the measured rotational diffusion of the coumarin dye probe. If we assume hydrodynamic orientational diffusion for a spherical body the size of the random coil (we take the average of the random coil diameters from SANS and DLS), the Stokes−Einstein−Debye hydrodynamic law permits us to estimate that the random coil would reorient on a time scale of 16 ns assuming a dilute room temperature aqueous polymer solution with a waterlike viscosity (1 cP). In addition, if the micelle were assumed to be rigid, then the predicted reorientation time constant for the entire micelle would be approximately 637 ns. If the interior were able to rotate independently of the entire micelle, it would have a rotational diffusion time of 130 ns. These predicted rotational time constants are all much longer than the longest time constants that we observed in our fluorescence depolarization experiments with the coumarin probes. These predicted time

constants are larger by a factor of ~4 for the random coil and by a factor of ~150 for the micellar aggregate. Further, from our test fits to simulated TCSPC data, we have determined that we are able to resolve long reorientational time constants on the order of 50 to 250 ns. Thus, we can immediately establish that each of the coumarin probes is localized in a flexible environment in the random coil, micelle, and micellar hydrogel phases.

From rheology measurements of 25 wt % Pluronic F88 performed by Brown et al.,[26] we estimate a dynamic viscosity[79] of approximately 5×10^7 cP at 55 °C for the hydrogel. We obtained a value of 4.5 cP for 25 w/v % F88 unimer solutions at 2.5 °C from our own previous shear viscosity measurements using an oscillating piston viscometer.[25] The hydrogel dynamic viscosity is several orders of magnitude larger than what is experienced by each one of the three coumarin dye probes. These results at first seem rather surprising, in that the hydrogel phase displays macroscopic properties consistent with being a solid, yet each of the three coumarin probes experiences complete fluorescence depolarization, albeit with widely varying rates. However, when one considers that although the gel is arguably a solid (with no creep upon inversion after several minutes),[22] the microscopic environment does not behave in any way like a solid. The environment may be waterlike as for $C343^-$ or PPO-like as for C153, or the probe may even span different regions of the aggregate as for C102.

Horng et al. derived empirical relationships between local friction and average rotation times for C153 solutions in both hydrogen bonded/polar and nonpolar solvents.[35] The relationship between local friction and reorientation is given by in the following equations

$$\langle\theta_{rot}\rangle_{polar} = 58\eta^{0.96} \quad (7)$$

$$\langle\theta_{rot}\rangle_{nonpolar} = 34.8\eta^{0.63} \quad (8)$$

$\langle\theta_{rot}\rangle_{polar}$ is the amplitude-weighted average rotational time constant in picoseconds for C153 in polar or hydrogen bonded liquids, while $\langle\theta_{rot}\rangle_{nonpolar}$ is the average rotation time in picoseconds for C153 in a nonpolar solvent, and η is the macroscopic shear viscosity in cP. Using these empirical equations and extrapolating to the average reorientation times that we have observed, we attempt to estimate the local viscosity for C153 in both the low temperature unimer (polar) regions as well as the micellar high temperature (nonpolar) region. We define the polar region as the temperature range for which the C153 steady-state emission spectrum is centered approximately at 546 nm. The nonpolar regime is defined as the temperature range for which the steady-state spectrum is centered at 521 nm.[25] For C153 in the polar region, the local friction experienced by the probe is approximately 4.7−6.7 cP for the 5 w/v % aqueous Pluronic F88 solution and 15−20 cP for the 25 w/v % solution. For the nonpolar micelle core region, the microviscosity ranges between approximately 198 cP at 38 °C to 14 cP at 90 °C for the 5 w/v % solution. For the 25 w/v % solution, the viscosity ranges between ~888 cP at 27.5 °C and 17 cP at 90 °C.

We can expand the use of the equation calibrated for C153 to the other two coumarins. We justify the use of the empirical relationship by noting that C102 and $C343^-$ are of similar structure and volume to C153. As shown in Table 1, the largest difference in molecular volumes does not exceed 6%. The equilibrium between the C343 neutral acid and the $C343^-$ is biased strongly in favor of the anion, so hydrogen bond donation from the C343 neutral acid does not lengthen the reorientation time noticeably, as would be the case for a solution of the C343 neutral acid in a nonaqueous but hydrogen bond accepting solvent such as DMSO.[80] $C343^-$ is highly water soluble and is presumed to be in a very waterlike and polar environment, which is consistent with the observed excitation and emission spectra. By using only eq 7 (for polar solvents) for $C343^-$, we get excellent agreement between macroscopic viscosity and the local viscosity experienced by the probe on the microscopic scale. From this result, we conclude that eq 7 should hold for $C343^-$ after a correction for the relative molecular volume ratio between C153 and $C343^-$. We can also calculate a local friction for C102. At 32 °C in aqueous F88 5 w/v % (the polar regime), the estimated microviscosity is 3.7 cP, while at 40 °C (the nonpolar regime) a value of 58 cP is obtained. The microviscosity experienced by C102 in the 25 w/v % F88 is estimated to be 8.7 cP at 20 °C and 174 cP at 28 °C.

TABLE 1: Calculated Logarithm of the Octanol−Water Partition Coefficient (CLOGP) and Molecular Volume Values for the Coumarins Used in This Study

coumarin	V (Å^3)[a]	CLOGP[b]
C153	245.5	4.081
C102	232.9	3.670
$C343^-$	239.7	−1.086

[a] Volumes calculated by the van der Waals increment method of Edwards.[81] [b] CLOGP values calculated from the method of ref 66.

The temperature profiles for the average reorientational responses of each of the three coumarin probes in the Pluronic F88 solutions are non-Arrhenius because of the presence of one or more phase transitions across the temperature range. However, over a restricted temperature range for which only a single solution phase is displayed, the average reorientational dynamics do display an Arrhenius behavior. Considering the unimer temperature range from 2.5 to 23 °C for the 5 w/v % Pluronic F88 solution, the activation energies for reorientation of C153, C102, and $C343^-$ are in the range from 3.5 to 5.5 kcal/mol. In the micellar phase, the Arrhenius energy values for C153 and C102 increase to 8.4 and 6.5 kcal/mol, respectively. A similar trend is also observed for the 25 w/v % Pluronic F88 solutions. The precipitous decrease in the average reorientation time constant above the cmT for both C153 and C102 is evidence for a different microenvironment relative to that of the unimer solution as reflected in the different Arrhenius activation energy for reorientation.

Two-Exponential Fluorescence Anisotropy Analysis vs Temperature. The parameters obtained from the two-exponential fluorescence anisotropy analysis are plotted vs temperature in Figures 5 and 6. For each of the these figures, the two reorientation time constants $\theta_{1,rot}$ and $\theta_{2,rot}$ are plotted in the right portion of the figure (parts b, d, and f) with the corresponding amplitudes r_1 and r_2 plotted in the left (parts a, c, and e). Figure 5 is for C153, C102, and $C343^-$ in 5 w/v% F88 solutions. Figure 6 shows the corresponding graphs for the 25 w/v% F88 aqueous solutions. We note that the measured fundamental anisotropy value r_0 is less than 0.373 in polar solvents and 0.378 in nonpolar solvents[35] because of the limits of the TCSPC instrument time resolution. This feature is common to the anisotropy parameters obtained for each of the dyes in both concentrations of F88 solutions and implies that a fraction of the fastest part of the reorientation dynamics is missed in our experiments.

In the discussion below, we will interpret the results of the two-exponential anisotropy analysis in terms of a two-site model, that is, each of the two amplitude fractions r_1 and r_2 and the

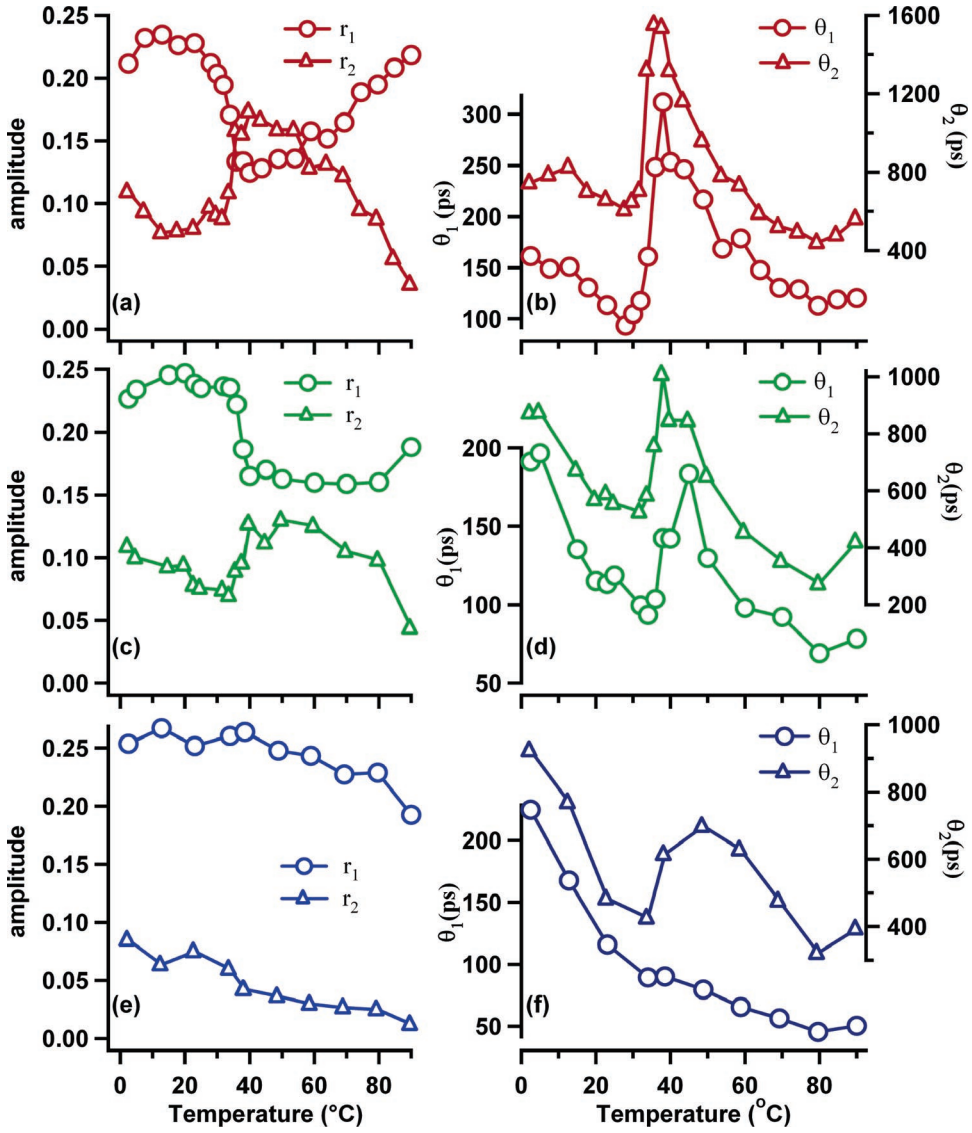

Figure 5. Two-exponential fluorescence anisotropy fit parameters plotted vs temperature for three coumarins in 5 w/v% aqueous F88 solutions. (a) Raw anisotropy amplitudes r_1 and r_2 for C153 vs temperature. (b) Time constants $\theta_{1,\mathrm{rot}}$ and $\theta_{2,\mathrm{rot}}$ for the C153 anisotropy decay (in picoseconds) vs temperature. (c) Raw anisotropy amplitudes r_1 and r_2 for C102 vs temperature. (d) Time constants $\theta_{1,\mathrm{rot}}$ and $\theta_{2,\mathrm{rot}}$ for the C102 anisotropy decay (in picoseconds) vs temperature. (e) Raw anisotropy amplitudes r_1 and r_2 for $C343^-$ vs temperature. (f) Time constants $\theta_{1,\mathrm{rot}}$ and $\theta_{2,\mathrm{rot}}$ for the $C343^-$ anisotropy decay (in picoseconds) vs temperature.

corresponding orientational relaxation time constants $\theta_{1,\mathrm{rot}}$ and $\theta_{2,\mathrm{rot}}$ will be assumed to probe a distinct environment. The amplitudes r_1 and r_2 corresponding to $\theta_{1,\mathrm{rot}}$ and $\theta_{2,\mathrm{rot}}$ for C153 in 5 w/v % F88 are shown in Figure 5a. The short time constant amplitude r_1 has a value of 0.21 at 2.5 °C and decreases to 0.13 at ~40 °C while the long time constant amplitude r_2 increases from 0.11 at 2.5 °C to 0.17 at 40 °C. The inversion point between r_1 and r_2 coincides with the increase in reorientation time constants and reflects the unimer-to-micelle phase transition. The amplitude for the longer reorientation time constant r_2 continues to decrease with increasing temperature to a value of 0.04 while r_1 increases to a value of 0.22 at 90 °C. The two amplitudes cross once again at approximately 55 °C indicating a relative shift in population fractions between microenvironments with increasing temperature.

For C153 in 5 w/v % F88, as displayed in Figure 5b, the double-exponential anisotropy fit displays short ($\theta_{1,\mathrm{rot}}$) and long ($\theta_{2,\mathrm{rot}}$) reorientation time constants differing by a factor of 4. Each of the reorientation time constants for C153 in 5 w/v % F88 decreases with increasing temperature over the range from 2.5 to 28 °C. The time constant $\theta_{2,\mathrm{rot}}$ decreases from 747 ps at 2.5 °C to 608 ps at 28 °C (except with a small increase to 827 ps at 13 °C), while over the same temperature range the time constant $\theta_{1,\mathrm{rot}}$ decreases from 161 to 94 ps. Both $\theta_{1,\mathrm{rot}}$ and $\theta_{2,\mathrm{rot}}$ then increase significantly to 312 and 1540 ps at 38 °C, respectively. From 38 to 90 °C, $\theta_{2,\mathrm{rot}}$ drops to 442 ps at 80 °C and then slightly increases to 564 ps at 90 °C. The short time constant $\theta_{1,\mathrm{rot}}$ decreases to 120 ps at 90 °C.

The variation of the anisotropy amplitudes with temperature for the C102 time constants in 5 w/v % F88 is shown in Figure 5c. The value of r_1 increases by about 10% from a value of 0.23 to 0.25 over the temperature range from 2.5 to 20 °C. Above 20 °C, the value of r_1 for C102 decreases to 0.17 at 40 °C, where it remains relatively constant with increasing temperature to 90 °C, where r_1 has increased to 0.19. The amplitude of the longer time constant r_2 behaves oppositely to r_1 except that it generally decreases to 0.07 at 40 °C from a value of 0.11 at 2.5 °C. At 40 °C, the value of r_2 for C102 has increased to 0.13 and then decreases steadily to 0.04 at 90 °C. While the C102 amplitudes do not cross as they do for C153 in 5 w/v %

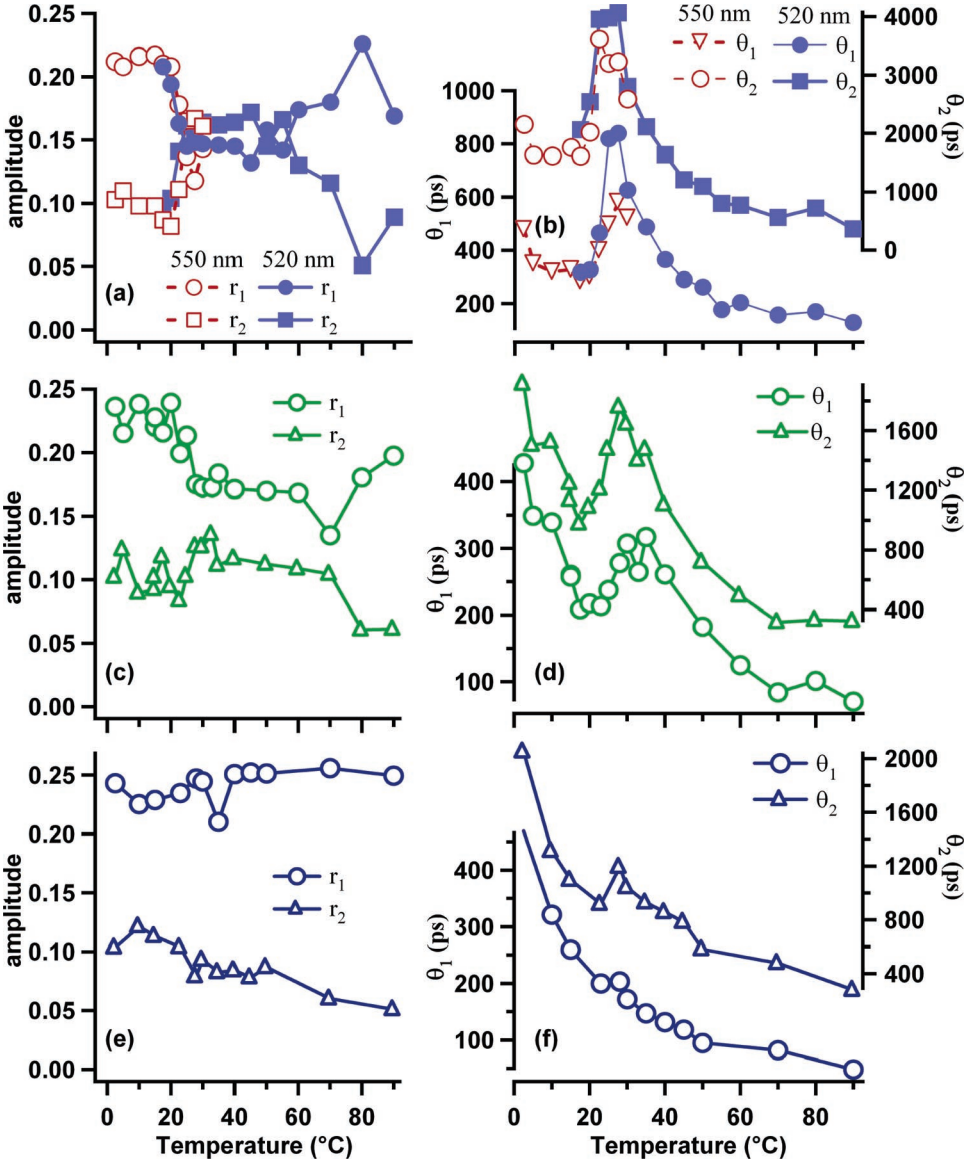

Figure 6. Two-exponential fluorescence anisotropy fit parameters plotted vs temperature for three coumarins in 25 w/v% aqueous F88 solutions. (a) Raw anisotropy amplitudes r_1 and r_2 for C153 vs temperature. (b) Time constants $\theta_{1,\mathrm{rot}}$ and $\theta_{2,\mathrm{rot}}$ for the C153 anisotropy decay (in picoseconds) vs temperature. (c) Raw anisotropy amplitudes r_1 and r_2 for C102 vs temperature. (d) Time constants $\theta_{1,\mathrm{rot}}$ and $\theta_{2,\mathrm{rot}}$ for the C102 anisotropy decay (in picoseconds) vs temperature. (e) Raw anisotropy amplitudes r_1 and r_2 for $C343^-$ vs temperature. (f) Time constants $\theta_{1,\mathrm{rot}}$ and $\theta_{2,\mathrm{rot}}$ for the $C343^-$ anisotropy decay (in picoseconds) vs temperature.

F88, they do converge toward one another at the same temperature where the time constants show their marked increase in reorientation times.

Figure 5d shows that, for C102 in 5 w/v % F88, the shorter $\theta_{1,\mathrm{rot}}$ and longer $\theta_{2,\mathrm{rot}}$ reorientation time constants decrease from 191 and 872 ps at 2.5 °C to 100 and 525 ps at 32 °C, respectively. The $\theta_{1,\mathrm{rot}}$ and $\theta_{2,\mathrm{rot}}$ graphs display maxima at different temperatures: 184 ps at 45 °C for the short time component $\theta_{1,\mathrm{rot}}$ and 1007 ps for the long time constant $\theta_{2,\mathrm{rot}}$ at 38 °C. The value of $\theta_{1,\mathrm{rot}}$ for C102 decreases to a value of 275 ps at 80 °C and then increases to 423 ps at 90 °C, while $\theta_{2,\mathrm{rot}}$ decreases with increasing temperature to a value of 78 ps at 90 °C.

Figure 5e shows that there is no inversion or even convergence of the $C343^-$ amplitudes, in contrast to the cases of C153 and C102. The time constant amplitudes r_1 and r_2 both decrease with increasing temperature from 0.25 and 0.08 at 2.5 °C to 0.19 and 0.01 at 90 °C, respectively. The amplitude for the faster reorientation time constant r_1 for $C343^-$ is the dominant fraction over the entire 2.5 to 90 °C range. The reorientation time constants for $C343^-$ in 5 w/v % F88 are shown in Figure 5f. The value of $\theta_{1,\mathrm{rot}}$ decreases steadily from 225 ps at 2.5 °C to 50 ps at 90 °C. In contrast, the long time component $\theta_{2,\mathrm{rot}}$ decreases with increasing temperature from 924 ps at 2.5 °C to 426 ps at 34 °C. The value of $\theta_{2,\mathrm{rot}}$ then increases to 698 ps at 49 °C followed by a decrease to 393 ps at 90 °C.

The values of the anisotropy amplitudes for coumarin 153 in aqueous 25 w/v % F88 are displayed in Figure 6a. The results are shown for TCSPC emission experiments measured at both 520 and 550 nm. Both wavelengths were monitored over the phase-transition region to determine that there was no significant deviation in trend of reorientation lifetime as a function of emission wavelength. The value of $r_1^{550\mathrm{nm}}$ for C153 at 2.5 °C is 0.21 and remains fairly constant until 22.5 °C where it decreases to a minimum of 0.12 at 28 °C. The value of $r_2^{550\mathrm{nm}}$ also shows a similar behavior with an initial value of 0.10 at 2.5 °C that decreases to 0.08 at 20 °C and then increases to 0.17 at 28 °C. The two 550 nm emission anisotropy amplitudes

r_1^{550nm} and r_2^{550nm} cross over at the temperature where there is an increase in reorientation times. Similarly, r_1^{520nm} has a value of 0.21 at 17.5 °C and decreases to a value of 0.15 and remains approximately constant with temperature until about 55 °C where it starts to increase, having a value of 0.17 at 90 °C. The value of r_2^{520nm} follows an opposite trend starting at 0.098 at 17.5 °C and then increasing to a value 0.16 at 27.5 °C. The amplitude remains relatively constant until 55 °C where r_2^{520nm} starts to decrease toward a value of 0.089 at 90 °C. As described above, the amplitudes display a relative inversion over the same temperature range that the reorientation time constants show a dramatic increase, which is a signature of the unimer-to-micelle phase transition.

Figure 6b shows the individual reorientation time constants for the double-exponential fits to the C153 anisotropies in the 25 w/v % F88 solution. It is immediately evident that the reorientation time constants for both emission wavelengths are strongly correlated. The shorter 550 nm emission time constant $\theta_{1,rot}^{550nm}$ decreases to 283 ps at 17.5 °C from 478 ps at 2.5 °C. The longer 550 nm emission time constant $\theta_{2,rot}^{550nm}$ decreases from 2155 ps at 2.5 °C to 1611 ps at 17.5 °C. The values of $\theta_{1,rot}^{550nm}$ display an increase to 581 ps but peak at 28 °C and decrease to 521 ps at 30 °C. The C153 reorientation time constant $\theta_{2,rot}^{550nm}$ also displays a dramatic increase to a maximum of 3614 ps at 23 °C and then sharply decreases to 2589 ps at 30 °C. Similar behavior is exhibited by the emission anisotropy detected at 520 nm, for which the shorter time constant $\theta_{1,rot}^{520nm}$ has a value of 317 ps at 17.5 °C but increases to 840 ps at 28 °C. For temperatures above 30 °C, $\theta_{1,rot}^{520nm}$ decreases rapidly with increasing temperature to 129 ps at 90 °C. The longer time constant $\theta_{2,rot}^{520nm}$ has value of 2063 ps at 17.5 °C and increases to 4063 ps at 28 °C. Above 25 °C, $\theta_{2,rot}^{520nm}$ decreases rapidly with increasing temperature to a value of 354 ps at 90 °C.

The values of the anisotropy amplitudes vs temperature for C102 in aqueous 25 w/v % F88 are shown in Figure 6c. The value of r_1 decreases with increasing temperature from 0.24 to 0.17 over the range from 2.5 to 28 °C, with the value of r_2 increasing from 0.10 to 0.13 over the same temperature range. Both amplitudes decrease with increasing temperature up to 70 °C; above 70 °C, r_1 increases to 0.20, and r_2 decreases to 0.06 at 90 °C.

Figure 6d shows the double-exponential anisotropy time constants vs temperature for C102 in 25 w/v % aqueous F88 solution. The value of $\theta_{1,rot}$ shows a decrease similar to that for C153, from 428 ps at 2.5 °C to 217 ps at 17.5 °C, whereas $\theta_{2,rot}$ decreases from 1913 ps at 2.5 °C to 977 ps at 17.5 °C. Both time constants increase over the temperature region from 17.5 to 30 °C with $\theta_{1,rot}$ reaching a maximum of 307 ps at 30 °C and $\theta_{2,rot}$ reaching a maximum of 1760 ps at 28 °C. Above 30 °C, both $\theta_{1,rot}$ and $\theta_{2,rot}$ decrease rapidly to a minimum of 324 and 70 ps at 90 °C, respectively.

Graphs of the fluorescence anisotropy fit parameters for the $C343^-$ in 25 w/v % F88 are shown in parts e and f of Figure 6. The amplitudes r_1 and r_2 are displayed in Figure 6e. The value of r_1 increases slightly over the temperature range from 2.5 to 90 °C from 0.24 to a final value of 0.25, while r_2 shows a slight decrease over the same temperature range starting at a value of 0.1 at 2.5 °C and ending at 0.05 at 90 °C. Figure 6f shows that the short time constant $\theta_{1,rot}$ for $C343^-$ has a value of 469 ps at 2.5 °C, while the longer time constant $\theta_{2,rot}$ has a value of 2052 ps at 2.5 °C. The values for both $C343^-$ reorientation time constants $\theta_{1,rot}$ and $\theta_{2,rot}$ decrease steadily to 917 and 200 ps at 23 °C, respectively. Above 28 °C, the value of $\theta_{1,rot}$ continues to decrease with increasing temperature to a value of 48 ps at 90 °C, whereas $\theta_{2,rot}$ increases to a maximum of 1194 ps at 28 °C and then subsequently decreases to 279 ps at 90 °C.

Detailed examination of the double-exponential fits yields some insight into the physical environment of the dye probes in the triblock copolymer aggregates. Upon examining the detailed analysis of the reorientational dynamics for $C343^-$ in the 5 w/v % aqueous F88, we see an interesting trend. The shorter $C343^-$ reorientation time constant $\theta_{1,rot}$ has little sensitivity to the microphase transition from unimers to micelles, while it appears that the longer time constant $\theta_{2,rot}$ has some small sensitivity to this transition. It should be pointed out that the temperature at which the rotational time constant increases in value is displaced to a higher temperature relative to the behavior of both C153 and C102. Further examination of the $C343^-$ reorientation amplitudes shows that the major fraction of the amplitude is in the shorter time constant. The relative amplitudes of the anisotropy decays correspond to the relative populations for the partitioning of $C343^-$ into different microenvironments. This is supported by our previous time-integrated spectra,[25] which showed that $C343^-$ was only weakly sensitive to the microphase transition. Further support for a model invoking two different environments comes from the fact that Stokes−Einstein−Debye hydrodynamic scaling behavior is observed for $C343^-$, that is, that the short time constant scales approximately with the measured macroscopic viscosity,[25] leading us to conclude that there is little association with the micelles for $C343^-$. $C343^-$ reorientational dynamics are very similar for both the 5 and 25 w/v % aqueous F88 solutions, further increasing the likelihood that most of the $C343^-$ population senses a bulk-like water environment.

Now we consider the complex reorientational behavior of C153 in the 5 w/v % aqueous F88 solution. Much like the case for $C343^-$, we assert that C153 resides in two distinct environments in the PPO core. Considering the time constants from the double-exponential fit to the polarization anisotropy decay, we find that both the shorter and longer rotational time constants $\theta_{1,rot}$ and $\theta_{2,rot}$ are sensitive to the micellization transition, because there is an increase to significantly longer rotational time constants over a fairly narrow temperature range near the cmT. However, we note that the difference in rotation time constants may reflect the type of environment. For example, the shorter time constant $\theta_{1,rot}$ for C153 is likely associated with the PPO/PEO interface or a more water-rich environment, while the longer time constant $\theta_{2,rot}$ is likely best assigned to the C153 dye probe being localized within the central PPO core of the micelle for temperatures above the cmT. The center of the PPO core is likely more viscous than the interface, which is adjacent to the more flexible water-rich PEO region, so the local friction experienced by the fluorescence probe may be reduced. Also, the shorter time constant $\theta_{1,rot}$ is shifted to slightly higher temperatures than the longer time constant, indicating that those C153 molecules have a different environment than the C153 molecules associated with the longer time constant $\theta_{2,rot}$. Another interesting observation is that the reorientation amplitudes (or relative populations) invert for temperatures near to the cmT. This appears to be consistent with the fact that at low temperatures there is a significant amount of water hydrating the PEO−PPO−PEO unimers. Once the temperature is raised beyond the cmT and the C153 is driven into the micelle, the populations should change since nearly all the water is excluded from the PPO block. It is well-known that structural changes from spherical to rodlike micelles occur for aqueous F88 solutions at temperatures above 90 °C,[7] so this second phase

transition could also contribute to the change in populations. The same arguments can be applied to the C153 orientational dynamics at the gel forming concentration in 25 w/v % aqueous F88.

The behavior of the C102 reorientational dynamics for both F88 concentrations is very similar to that for C153 except that the temperature response of the time constants $\theta_{1,\mathrm{rot}}$ and $\theta_{2,\mathrm{rot}}$ is shifted to higher temperatures by about 2−5 °C for C102 for both F88 concentrations. The temperature-dependent behavior of the C102 amplitudes r_1 and r_2 is similar to that for C153 with one slight difference. The amplitudes converge with increasing temperature, but do not cross, and with increasing temperature, the amplitudes reverse direction. This may indicate that there is a similar shift in environmental population with temperature. The amplitudes for C102 reorientational dynamics in 5 and 25 w/v % aqueous F88 both display this behavior.

Jeon et al. employed the cationic dye probe rhodamine 123 ($R123^+$) to study local friction in aqueous solutions of a related PEO−PPO−PEO triblock copolymer, Pluronic F127.[22] The $R123^+$ probe is surprisingly hydrophobic (CLOGP[66] value of 1.51) considering that it is a cation. Jeon et al. found that the $R123^+$ fluorescence anisotropy decay was double exponential in nature. The double-exponential nature of the probe reorientation was attributed to partitioning of $R123^+$ into two regions with different microenvironments. One reorientation time constant was associated with the bulk water, much like our $C343^-$, and the other $R123^+$ reorientation was associated with the micelle but outside of the micelle core. The interesting difference between the work of Jeon et al.[22] and the present work with coumarins is that the reorientation time constants assigned to association of $R123^+$ with the micelle were sensitive to the gelation point of the F127 triblock copolymer. The $C343^-$ is only slightly sensitive to the microphase transition to form micelles in the Pluronic F88 solutions and is insensitive to the micelle-to-hydrogel phase transition. Jeon et al. postulated that $R123^+$ is sensitive to the gelation point of F127 solutions because it is a cation. The reason that $R123^+$ is sensitive to the gelation and $C343^-$ is sensitive to the micellization could be as simple as the difference in the sign of the charge, that is, cation vs anion. Details of the charge distribution for $R123^+$ and $C343^-$ may yield clues about the origin of this effect. For example, electronic structure calculations reveal that the charge on the $C343^-$ mainly resides on the carboxylate, while for $R123^+$ the positive charge is delocalized more evenly across the ring system. Small cations may form specific chelating bonds with polyether oxygen atoms that will not occur for anions. It is not clear that larger cationic probes such as $R123^+$ can associate with the polyether oxygens in the same way.

The detailed analyses of the fluorescence anisotropy data discussed above imply that there is a fraction of C153 that resides in a microenvironment that has a smaller local friction than that for some fraction of C102. A similar trend is seen for $C343^-$ where a small fraction experiences a larger local friction than some fraction of C102 and C153. However, we do observe that the relative fractions (amplitudes) of C102 and $C343^-$ are smaller than the fractions (amplitudes) for C153 for a given value of the time constant. In other words, the fraction of C153 molecules that experience a large local friction is greater than the fractions for the C102 and the $C343^-$. Conversely, the fraction of $C343^-$ molecules that experiences a small local friction is on average larger than that for C102 and C153. The dipole jump in coumarins upon photoexcitation[32] leads to an emission red shift of 2000 to 4000 cm^{-1}, resulting from solvent and polymer motions in the surrounding environment. Thus, it is important to recognize that this nonequilibrium coumarin excited state may induce segmental motions in the PEO and/or PPO chains. It is likely that the fast time constant for rotation for the coumarin probes used here may be connected to polymer motions on time scales that permit rapid reorientation, while the longer rotational time constant may be connected to slower polymer motions. It should be noted that for the case of these triblock copolymers in the micellar aggregates, the time scales for solvation measured by the TDFSS method are on the order of the rotational correlation time constants. These comments are based on preliminary TDFSS experiments using C153 that we have performed on Pluronic F88 micelles, for which the solvation is highly nonexponential and spans the time range of tens of picoseconds to several nanoseconds. This explanation does not modify our previous assumption that the coumarin dyes partition into different regions of the aggregates, since we have shown previously by fluorescence lifetime and time-integrated spectroscopy that the dyes experience a significant change in polarity when the critical micelle temperature is exceeded. The relative hydrophobicities for each of the three coumarin probes and their relative solubilities make a strong case for such partitioning. Ongoing solvation dynamics experiments for several Pluronic systems will further elucidate the physical nature of these phenomena.

Conclusions

Fluorescence anisotropy studies using three different coumarin fluorescence probes having a broad range of hydrophobicity have been used to investigate the local friction in aqueous solutions of triblock copolymers. The PEO−PPO−PEO triblock copolymers are nonionic surfactants that are highly water soluble and at elevated temperatures form spherical micelles. At still higher concentrations, the spherical micelles can form body centered cubic (bcc) hydrogels. We have investigated the microviscosity in different regions of the aqueous polymer solutions by comparing the rotational correlations obtained for the coumarins having substantially different hydrophobic properties.

The fluorescence anisotropy results permit detailed comparisons to be made between the measured microviscosities, macroscopic shear viscosities, and dynamic viscosities for these solutions. Through the use of three coumarin probes, microviscosities have been estimated to range from 4 to 900 cP for the different environments in the F88 triblock copolymer unimer and aggregate solutions, while the dynamic shear viscosity ranges from 4 cP (unimer solution) to in excess of 5×10^7 cP for the 25 w/v % hydrogel environment. This represents a peak ratio of 50 000 between the microscopic and macroscopic viscosities for this system in the hydrogel phase. Reorientational friction for unimer solutions of aqueous F88 has been shown to correlate with hydrodynamic scaling laws. The observed average reorientation time constants are found to precisely track the unimer-to-micelle microphase transitions previously observed using fluorescence excitation and emission shifts and lifetimes.[25] However, unlike the results of Jeon et al.,[22] we find that there is no observable feature in the reorientation time constant vs temperature response profile at the gelation temperature. In this work, we believe that we have sampled the local friction for all of the relevant microenvironments including waterlike, random coil unimer solution, wet PEO, PEO−PPO interface, and dry PPO micellar cores. Ongoing work focuses on understanding both the microviscosities and the time-dependent fluorescence Stokes shift behaviors for the same F88 polymer solutions, as well as other micellar, rodlike micellar, cubic, hexagonal, and lamellar phases.

In this paper, we hope to have achieved two goals. First, we have used time-resolved fluorescence anisotropy for three coumarin probes, each having substantially different hydrophobicities, to explore the local friction in two concentrations of aqueous PEO−PPO−PEO triblock copolymer solutions. In these fluorescence anisotropy experiments, we have explored the friction for unimer, micellar, and micellar hydrogel solutions by varying the temperature over the range from 2.5 to 90 °C. Further, we have probed several solution regions including aqueous, PEO, PEO−PPO interface, and core PPO environments. A second goal has been to further extend the multiple hydrophobic probe methodology so that these same coumarins (or other combinations of chromophores with tunable hydrophobic properties) can be used to probe friction in other important solution aggregate environments. We will be continuing to expand this method for investigating the microviscosity in different regions of polymer solutions, porous nanomaterials, and especially the hydrophobic pockets of relevant biopolymers.

Acknowledgment. We gratefully acknowledge support from the National Science Foundation and the donors of the American Chemical Society Petroleum Research Fund. K.S. gratefully acknowledges support as a NSF IGERT fellow. We thank BASF for the gift of high-purity Pluronic F88. We thank Dr. Hideaki Shirota and Prof. David Talaga for helpful discussions. We also thank Benjamin Lee and Jason Giurleo for developing the simultaneous anisotropy fitting code in Igor Pro.

Supporting Information Available: The parameters obtained from nonlinear least-squares fitting of the fluorescence anisotropy data to eqs 2−6 are presented. This material is available free of charge via the Internet at http://pubs.acs.org.

References and Notes

(1) Alexandridis, P.; Nivaggioli, T.; Hatton, T. A. *Langmuir* **1995**, *11*, 1468.
(2) Kabanov, A. V.; Nazarova, I. R.; Astafieva, I. V.; Batrakova, E. V.; Alakhov, V. Y.; Yaroslavov, A. A.; Kabanov, V. A. *Macromolecules* **1995**, *28*, 2303.
(3) Rapoport, N. *Colloids Surf., B* **1999**, *16*, 93.
(4) Scherlund, M.; Welin-Berger, K.; Brodin, A.; Malmsten, M. *Eur. J. Pharm. Sci.* **2001**, *14*, 53.
(5) Alexandridis, P.; Hatton, T. A. *Colloids Surf., A* **1995**, *96*, 1.
(6) Alexandridis, P.; Olsson, U.; Lindman, B. *Langmuir* **1998**, *14*, 2627.
(7) Schillen, K.; Brown, W.; Johnsen, R. M. *Macromolecules* **1994**, *27*, 4825.
(8) Wanka, G.; Hoffmann, H.; Ulbricht, W. *Macromolecules* **1994**, *27*, 4145.
(9) Aswal, V. K.; Goyal, P. S.; Kohlbrecher, J.; Bahadur, P. *Chem. Phys. Lett.* **2001**, *349*, 458.
(10) Goldmints, I.; von Gottberg, F. K.; Smith, K. A.; Hatton, T. A. *Langmuir* **1997**, *13*, 3659.
(11) Goldmints, I.; Yu, G. E.; Booth, C.; Smith, K. A.; Hatton, T. A. *Langmuir* **1999**, *15*, 1651.
(12) Jain, N. J.; Aswal, V. K.; Goyal, P. S.; Bahadur, P. *J. Phys. Chem. B* **1998**, *102*, 8452.
(13) Mortensen, K.; Brown, W. *Macromolecules* **1993**, *26*, 4128.
(14) Walderhaug, H. *J. Phys. Chem. B* **1999**, *103*, 3352.
(15) Walderhaug, H.; Nystroem, B. *J. Phys. Chem. B* **1997**, *101*, 1524.
(16) Brown, W.; Schillen, K.; Almgren, M.; Hvidt, S.; Bahadur, P. *J. Phys. Chem.* **1991**, *95*, 1850.
(17) Yu, G.; Altinok, H.; Nixon, S. K.; Booth, C.; Alexandridis, P.; Hatton, T. A. *Eur. Polym. J.* **1997**, *33*, 673.
(18) Alexandridis, P.; Holzwarth, J. F.; Hatton, T. A. *Macromolecules* **1994**, *27*, 2414.
(19) Armstrong, J.; Chowdhry, B.; Mitchell, J.; Beezer, A.; Leharne, S. *J. Phys. Chem.* **1996**, *100*, 1738.
(20) Wanka, G.; Hoffmann, H.; Ulbricht, W. *Colloid Polym. Sci.* **1990**, *268*, 101.
(21) Guo, C.; Wang, J.; Liu, H.-z.; Chen, J.-y. *Langmuir* **1999**, *15*, 2703.
(22) Jeon, S.; Granick, S.; Kwon, K. W.; Char, K. *J. Polym. Sci., Part B: Polym. Phys.* **2002**, *40*, 2883.
(23) Nivaggioli, T.; Alexandridis, P.; Hatton, T. A.; Yekta, A.; Winnik, M. A. *Langmuir* **1995**, *11*, 730.
(24) Nivaggioli, T.; Tsao, B.; Alexandridis, P.; Hatton, T. A. *Langmuir* **1995**, *11*, 119.
(25) Grant, C. D.; DeRitter, M. R.; Steege, K. E.; Fadeeva, T. A.; Castner, E. W., Jr. *Langmuir* **2005**, *21*, 1745.
(26) Brown, W.; Schillen, K.; Hvidt, S. *J. Phys. Chem.* **1992**, *96*, 6038.
(27) Mortensen, K. *J. Phys.: Condens. Matter* **1996**, *8*, A103.
(28) Mortensen, K.; Brown, W.; Norden, B. *Phys. Rev. Lett.* **1992**, *68*, 2340.
(29) Almgren, M.; Bahadur, P.; Jansson, M.; Li, P.; Brown, W.; Bahadur, A. *J. Colloid Interface Sci.* **1992**, *151*, 157.
(30) Kositza, M. J.; Bohne, C.; Alexandridis, P.; Hatton, T. A.; Holzwarth, J. F. *Macromolecules* **1999**, *32*, 5539.
(31) Nakashima, K.; Takeuchi, K. *Appl. Spectrosc.* **2001**, *55*, 1237.
(32) Cave, R. J.; Castner, E. W., Jr. *J. Phys. Chem. B* **2002**, *106*, 12117.
(33) Sulpizi, M.; Carloni, P.; Hutter, J.; Rothlisberger, U. *Phys. Chem. Chem. Phys.* **2003**, *5*, 4798.
(34) Sulpizi, M.; Rohrig, U. F.; Hutter, J.; Rothlisberger, U. *Int. J. Quantum Chem.* **2005**, *101*, 671.
(35) Horng, M. L.; Gardecki, J. A.; Maroncelli, M. *J. Phys. Chem. A* **1997**, *101*, 1030.
(36) Horng, M. L.; Gardecki, J. A.; Papazyan, A.; Maroncelli, M. *J. Phys. Chem.* **1995**, *99*, 17311.
(37) Barbara, P. F.; Jarzeba, W. *Adv. Photochem.* **1990**, *15*, 1.
(38) Cave, R. J.; Burke, K.; Castner, E. W., Jr. *J. Phys. Chem. A* **2002**, *106*, 9294.
(39) Chowdhury, A.; Locknar, S. A.; Premvardhan, L. L.; Peteanu, L. A. *J. Phys. Chem. A* **1999**, *103*, 9614.
(40) Matyushov, D. V.; Newton, M. D. *J. Phys. Chem. A* **2001**, *105*, 8516.
(41) Argaman, R.; Huppert, D. *J. Phys. Chem. A* **1998**, *102*, 6215.
(42) Shirota, H.; Segawa, H. *J. Phys. Chem. A* **2003**, *107*, 3719.
(43) Corbeil, E. M.; Riter, R. E.; Levinger, N. E. *J. Phys. Chem. B* **2004**, *108*, 10777.
(44) Pant, D.; Levinger, N. E. *Langmuir* **2000**, *16*, 10123.
(45) Pant, D.; Riter, R. E.; Levinger, N. E. *J. Chem. Phys.* **1998**, *109*, 9995.
(46) Riter, R. E.; Undiks, E. P.; Kimmel, J. R.; Levinger, N. E. *J. Phys. Chem. B* **1998**, *102*, 7931.
(47) Riter, R. E.; Undiks, E. P.; Levinger, N. E. *J. Am. Chem. Soc.* **1998**, *120*, 6062.
(48) Riter, R. E.; Willard, D. M.; Levinger, N. E. *J. Phys. Chem. B* **1998**, *102*, 2705.
(49) Shirota, H.; Horie, K. *J. Phys. Chem. B* **1999**, *103*, 1437.
(50) Willard, D. M.; Riter, R. E.; Levinger, N. E. *J. Am. Chem. Soc.* **1998**, *120*, 4151.
(51) Corbeil, E. M.; Levinger, N. E. *Langmuir* **2003**, *19*, 7264.
(52) Sarkar, N.; Datta, A.; Das, S.; Bhattacharyya, K. *J. Phys. Chem.* **1996**, *100*, 15483.
(53) Pal, S. K.; Sukul, D.; Mandal, D.; Sen, S.; Bhattacharyya, K. *J. Phys. Chem. B* **2000**, *104*, 2613.
(54) Levinger, N. E. *Curr. Opin. Colloid Interface Sci.* **2000**, *5*, 118.
(55) Changenet-Barret, P.; Choma, C. T.; Gooding, E. F.; DeGrado, W. F.; Hochstrasser, R. M. *J. Phys. Chem. B* **2000**, *104*, 9322.
(56) Vajda, S.; Jimenez, R.; Rosenthal, S. J.; Fidler, V.; Fleming, G. R.; Castner, E. W., Jr. *J. Chem. Soc., Faraday Trans.* **1995**, *91*, 867.
(57) Bart, E.; Meltsin, A.; Huppert, D. *J. Phys. Chem.* **1994**, *98*, 3295.
(58) Das, K.; Sarkar, N.; Das, S.; Datta, A.; Bhattacharyya, K. *Chem. Phys. Lett.* **1996**, *249*, 323.
(59) Frauchiger, L.; Shirota, H.; Uhrich, K. E.; Castner, E. W., Jr. *J. Phys. Chem. B* **2002**, *106*, 7463.
(60) Arzhantsev, S.; Ito, N.; Heitz, M.; Maroncelli, M. *Chem. Phys. Lett.* **2003**, *381*, 278.
(61) Chakrabarty, D.; Harza, P.; Chakraborty, A.; Seth, D.; Sarkar, N. *Chem. Phys. Lett.* **2003**, *381*, 697.
(62) Chowdhury, P. K.; Halder, M.; Sanders, L.; Calhoun, T.; Anderson, J. L.; Armstrong, D. W.; Song, X.; Petrich, J. W. *J. Phys. Chem. B* **2004**, *108*, 10245.
(63) Ito, N.; Arzhantsev, S.; Heitz, M.; Maroncelli, M. *J. Phys. Chem. B* **2004**, *108*, 5771.
(64) Karmakar, R.; Samanta, A. *J. Phys. Chem. A* **2002**, *106*, 4447.
(65) Shirota, H.; Tamoto, Y.; Segawa, H. *J. Phys. Chem. A* **2004**, *108*, 3244.
(66) clogP calculator. Daylight Chemical Information Systems. http://www.daylight.com/daycgi/clogp.
(67) Shirota, H.; Castner, E. W., Jr. *J. Chem. Phys.* **2000**, *112*, 2367.
(68) Sun, Y.; Castner, E. W., Jr.; Lawson, C. L.; Falkowski, P. G. *FEBS Lett.* **2004**, *570*, 175.
(69) Lakowicz, J. R. *Principles of Fluorescence Spectroscopy*, 2nd ed.; Kluwer Academic: New York, 1999.
(70) Valeur, B. *Molecular Fluorescence: An Introduction- Principles and Applications*, 1st ed.; Wiley-VCH: Weinheim, Germany, 2001.

(71) Cross, A.; Fleming, G. *Biophys. J.* **1984**, *46*, 45.
(72) Wavemetrics, I. *Igor Pro*, 4.09A ed.; Wavemetrics, Inc.: Lake Oswego, OR, 2003.
(73) Maroncelli, M.; Fleming, G. R. *J. Chem. Phys.* **1987**, *86*, 6221.
(74) Kinosita, K.; Kawato, S.; Ikegami, A. *Biophys. J.* **1977**, *20*, 289.
(75) Lipari, G.; Szabo, A. *Biophys. J.* **1980**, *30*, 489.
(76) Jones, G., II; Jackson, W. R.; Choi, C.-y.; Bergmark, W. R. *J. Phys. Chem.* **1985**, *89*, 294.
(77) Pryor, B. A.; Palmer, P. M.; Andrews, P. M.; Berger, M. B.; Topp, M. R. *J. Phys. Chem. A* **1998**, *102*, 3284.
(78) Pryor, B. A.; Palmer, P. M.; Chen, Y.; Topp, M. R. *Chem. Phys. Lett.* **1999**, *299*, 536.
(79) Sperling, L. H. *Introduction to Physical Polymer Science*; John Wiley & Sons Inc.: New York, 1992.
(80) Dutt, G. B.; Ghanty, T. K. *J. Phys. Chem. B* **2003**, *107*.
(81) Edwards, J. T. *J. Chem. Educ.* **1970**, *47*, 261.